International Journal of Biological Macromolecules 183 (2021) 213–221

Contents lists available at ScienceDirect

International Journal of Biological Macromolecules

journal homepage: http://www.elsevier.com/locate/ijbiomac

Structural basis of the cooperative activation of type II citrate synthase (*Hy*CS) from *Hymenobacter* sp. PAMC 26554

Sun-Ha Park [a,1,2], Chang Woo Lee [a,c,1], Da-Woon Bae [b,1], Hackwon Do [a], Chang-Sook Jeong [a,c], Jisub Hwang [a,c], Sun-Shin Cha [b,*], Jun Hyuck Lee [a,c,**]

[a] Research Unit of Cryogenic Novel Material, Korea Polar Research Institute, Incheon 21990, Republic of Korea
[b] Department of Chemistry & Nanoscience, Ewha Womans University, Seoul 03760, Republic of Korea
[c] Department of Polar Sciences, University of Science and Technology, Incheon 21990, Republic of Korea

ARTICLE INFO

Article history:
Received 4 March 2021
Received in revised form 20 April 2021
Accepted 22 April 2021
Available online 25 April 2021

Keywords:
Crystal structure
Citrate synthase
Hymenobacter sp. PAMC 26554
Domain movement
X-ray crystallography

ABSTRACT

Citrate synthase (CS) catalyzes the formation of citrate and coenzyme A from acetyl-CoA and oxaloacetate. CS exists in two forms: type I and type II. We determined the citrate-bound crystal structure of type II CS from the *Hymenobacter* sp. PAMC 26554 bacterium (*Hy*CS; isolated from Antarctic lichen). Citrate molecules bound to a cleft between the large and small domains of *Hy*CS. Structural comparison of *Hy*CS with other type II CSs revealed that type II CSs have a highly conserved flexible hinge region (residues G264–P265 in *Hy*CS), enabling correct positioning of active site residues. Notably, the catalytic His266 residue of *Hy*CS interacted with Trp262 in the inactive (unliganded open) state of other type II CSs, whereas the His266 residue moved to the active site via a small-domain swing motion, interacting with the bound citrate in the closed conformation of *Hy*CS. However, type I CSs lack this tryptophan residue and face-to-edge interactions. Thus, type II CSs might have a unique domain-motion control mechanism enabling a tight allosteric regulation. An activity assay using a W262A mutant showed a Hill coefficient of 2.4; thus, the interaction between Trp262 and His266 was closely related to the positive cooperative ligand binding of type II CS.

1. Introduction

The citric acid cycle is a central metabolic pathway that conserves oxidation energy in the form of NADH and $FADH_2$, and provides 4- and 5-carbon intermediates as precursors for various molecules. Citrate synthase (CS EC 2.3.3.1) catalyzes the condensation of acetyl-coenzyme A (acetyl-CoA) and oxaloacetic acid (OAA) to form citrate, which is the first step in this cycle [1]. Because of their key role in the citric acid cycle, CSs are distributed in nearly all living organisms [2]. In particular, CSs are classified into two types, type I and type II, depending on their sources and oligomerization states. Type II CSs forming hexamers are distributed in gram-negative bacteria, whereas type I CSs are dimeric enzymes present in eukaryotes, gram-positive bacteria, and archaea [3].

To date, several type I and II CSs have been biochemically and structurally characterized. Monomers of both types have been reported to show 35–40% sequence similarity, with similar active sites harboring two histidines and an aspartate as catalytic residues [2,3]. The monomeric structure of CSs is commonly composed of a large and a small domain; generally, the large domain has 3 times more residues than the small domain. The small domain contains the catalytic aspartate residue and a single histidine residue, whereas the other catalytic histidine residue is located at the hinge loop connecting the two domains. The active site that accommodates both OAA and acetyl-CoA is situated at the cleft between the two domains. Monomeric CSs can interconvert between open (inactive) and closed (active) conformations. More specifically, OAA binds to the active site of CSs in the open conformation, transforming CSs to the closed conformation to create a binding site for acetyl-CoA [2,3]. Consequently, CSs have an ordered substrate-binding mode in which OAA binding is followed by acetyl-CoA binding. Compared with type I CSs, type II enzymes typically have additional N-terminal residues [1–3] that mediate tight dimer interactions. Although the dimeric conformation of type II CSs is similar to that of type I CSs, three dimers are assembled to form a hexamer; that is, a type II CS is a trimer of dimers. Some type II CS enzymes are allosterically regulated; they can be activated by several salts, such as KCl, and specifically inhibited by NADH, ATP, and citrate [4,5]. For example, type II CS from *Escherichia coli* (*Ec*CS) is allosterically inhibited by NADH [6,7]; the residues responsible for NADH binding are located along the dimer-dimer

* Corresponding author.
** Correspondence to: J. H. Lee, Research Unit of Cryogenic Novel Material, Korea Polar Research Institute, Incheon 21990, Republic of Korea.
E-mail addresses: chajung@ewha.ac.kr (S.-S. Cha), junhyucklee@kopri.re.kr (J.H. Lee).
[1] These authors contributed equally.
[2] Present address: Public CDMO for Microbial-based Vaccine, Infrastructure Project Organization for Global Industrialization of Vaccine, Hwasun, 58141, Republic of Korea.

https://doi.org/10.1016/j.ijbiomac.2021.04.141
0141-8130/

interface in the hexameric conformation, indicating that NADH is a non-competitive allosteric inhibitor. These findings explain why type I dimeric enzymes are not inhibited by NADH. Interestingly, the type II CS from the acid-tolerant bacterium *Acetobacter aceti* (*Aa*CS) lacks the NADH-binding residues and is thus insensitive to NADH inhibition [8].

In addition, previous studies have revealed that ligand binding to mutant *Ec*CS is regulated in a cooperative manner [9]. Cooperative ligand binding observed in multimeric enzymes is an inherent consequence of the communication between subunits via ligand-induced structural rearrangements. This communication provides a variety

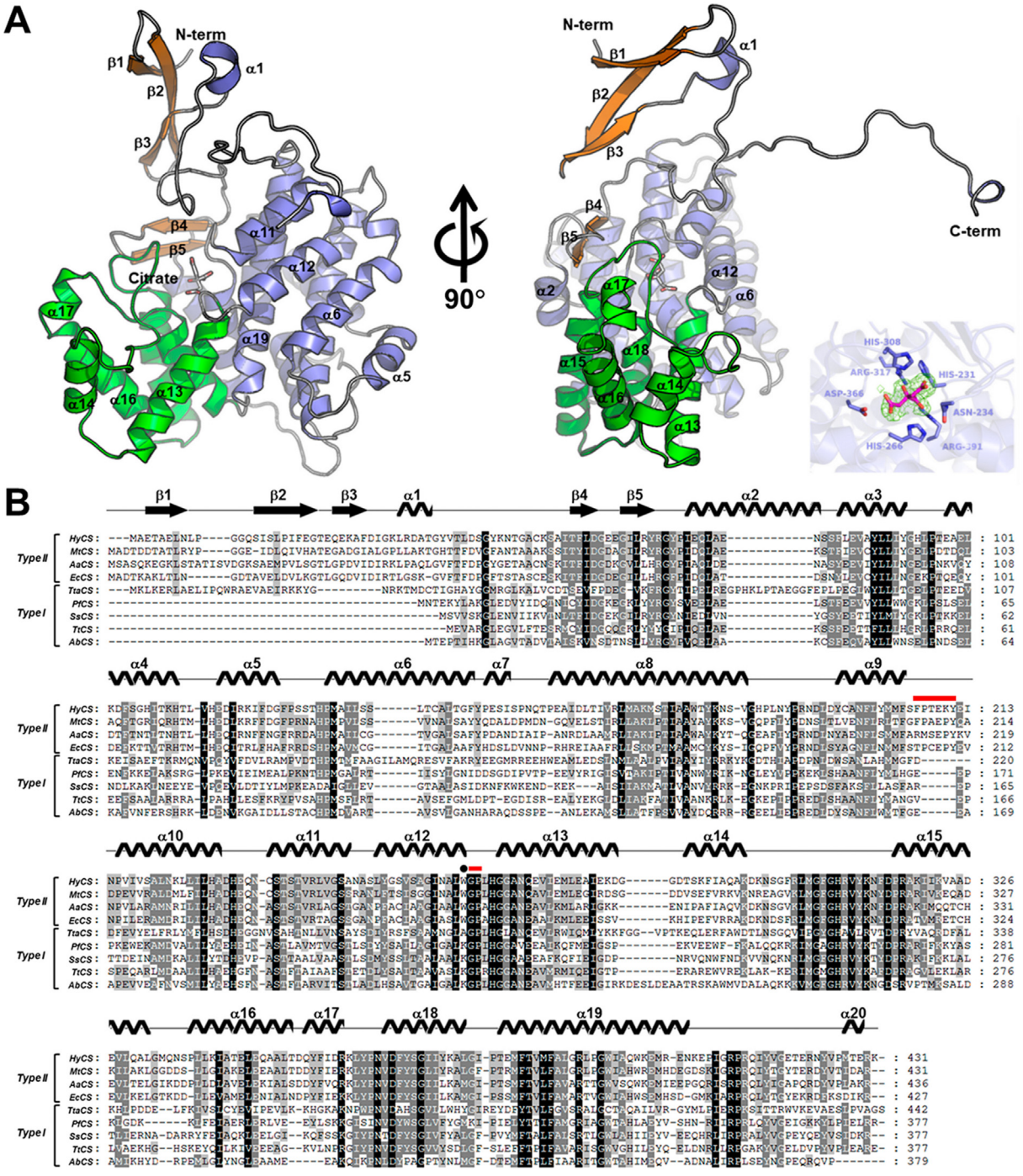

Fig. 1. Crystal structure of *Hy*CS and multiple sequence alignment of type I and type II CSs. (A) Monomer structure of *Hy*CS and 90° rotated view. The α-helices are shown in slate blue and green, whereas β-strands are shown in orange. The inset on the right shows the bound citrate molecule with the Fo-Fc omit map contoured at 3σ (green mesh). The citrate-interacting residues are represented as sticks. (B) Multiple amino acid sequence alignment of type II and type I CSs including sequences of *Hy*CS from *Hymenobacter* sp. PAMC 26554 (UniProtKB code: A0A142HAE2), *Mt*CS from *Mycobacterium tuberculosis* (PDB code: 4TVM; UniProtKB code: P9WPD5), *Aa*CS from *Acetobacter aceti* (PDB code: 2H12; UniProtKB code: P20901), *Ec*CS from *Escherichia coli* (PDB code: 4G6B; UniProtKB code: P0ABH7), *Tta*CS from *Thermosulfidibacter takaii* (UniProtKB code: A0A0S3QTD0), *Pf*CS from *Pyrococcus furiosus* (PDB code: 1AJ8; UniProtKB code: Q53554), *Ss*CS from *Sulfolobus solfataricus* (PDB code: 1O7X; UniProtKB code: P80148), *Tt*CS from *Thermus thermophilus* (PDB code: 1IOM; UniProtKB code: Q5SIM6), and *Ab*CS from *Antarctic bacterium* DS2-3R (PDB code: 1A59; UniProtKB code: O34002). The secondary structure elements of *Hy*CS are shown above the alignment. The highly conserved tryptophan residue in the type II CS group (Trp262 of *Hy*CS) is marked with a black circle. The conserved hinge-region residues (Gly263 and Pro264 of *Hy*ECH) and additional sequences of Type II CSs are marked with red bars.

of regulatory mechanisms and impacts both the kinetic and thermodynamic properties of multimeric proteins. However, the mechanism by which long-distance communication among different subunits and cooperative ligand binding for allosteric regulation are achieved in type II CSs remains unclear. To understand the structural basis of the allosteric regulation and cooperative ligand binding in type II CSs, we determined the crystal structure of *Hy*CS from the UV radiation-resistant bacterium, *Hymenobacter* sp. PAMC 26554, which was isolated from the Antarctic lichen. This is the first-ever structure of citrate-bound type II CS, which, together with site-directed mutagenesis and kinetic assays, presents a plausible mechanism for the tight allosteric control and cooperative ligand binding in *Hy*CS.

2. Results and discussion

2.1. Overall structure of HyCS

We determined the crystal structure of the citrate-bound type II *Hy*CS at 2.2 Å resolution using the molecular replacement method with the type II CS structure from *Mycobacterium tuberculosis* (*Mt*CS, PDB code 4TVM) as a search model [10,11] (Fig. 1). Although the

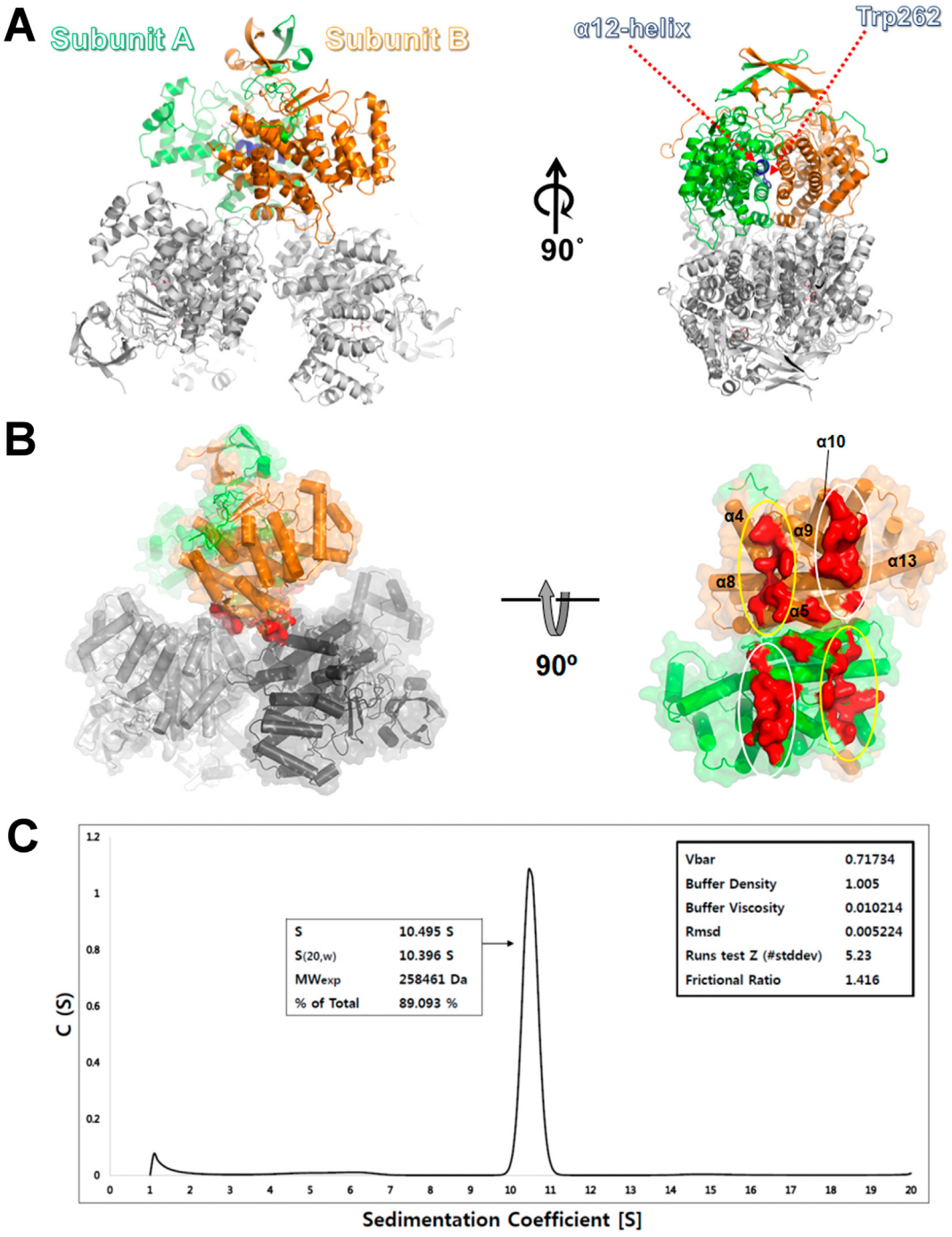

Fig. 2. Hexamerization of *Hy*CS. (A) Hexamer structure of *Hy*CS. The α12-helix is marked in slate blue color, with the Trp262 residue being presented in a stick model. (B) Overall hexameric structure of *Hy*CS formed from three dimers and binding interface. The contact residues of one dimer in the interaction interface within 5 Å of the two neighboring dimers are presented with red color (right panel). Sites I and II in the dimer-dimer interface are marked with white and yellow oval circles, respectively. (C) The analytical ultracentrifugation profile of *Hy*CS showed that this enzyme exists as a hexamer in solution.

asymmetric unit contained three molecules, we generated the hexameric structure (a trimer of dimers) of *Hy*CS using crystallographic symmetry (Fig. 2A and B). It should be noted that we confirmed the hexameric assembly of *Hy*CS using analytical ultracentrifugation (Fig. 2C). We found that the final model of the citrate-bound *Hy*CS contained 1290 amino acids and 394 water molecules with R_{work} and R_{free} values of 0.19 and 0.2235, respectively (Table 1). The overall structure of the *Hy*CS monomer was divided into large and small domains (Fig. 1). The large domain was composed of 14 α-helices (α1–α12 and α19–α20) and five β-strands (β1–β5 strands), whereas the small domain consisted of six α-helices (α13–α18). Acetyl-CoA and oxaloacetate bind to the cleft between the two domains.

The dimeric interactions of *Hy*CS were mediated by the N-terminal protrusion region (residues 1–54 including β1-β3 and α1) of the large domain, the four α-helices in the main body of the large domain (α5, α6, α11, and α12), and the C-terminal tail (residues 407–431). The N-terminal protrusion region was composed of a three-stranded β-sheet (β1–β3) and α1-helix. Two N-terminal protrusion regions from neighboring monomers were combined through the formation of an intermolecular β-sheet. Moreover, the β1 and β3 strands of a monomer were detected to be hydrogen-bonded to the β1 and β3 strands of the contacting monomer, respectively, forming a six-stranded intermolecular β-sheet (Fig. 2A). The four α-helices in the large domain of a monomer interacted with the corresponding α-helices of the contacting monomer in a head-to-tail manner. For example, the amino (or carboxyl)-terminal end of α11 in a monomer appeared to face the carboxyl (or amino)-terminal end of the same helix in the contacting monomer, thus allowing for electrostatic interactions between oppositely charged helix dipoles. We also noted that the C-terminal tail of a monomer stretched over the contacting monomer bridging the N-terminal protrusion region and the main body of the large domain in the contacting monomer. Accordingly, through this swapping interaction mode, the C-terminal tail of a monomer participated in the constitution of the active site in the contacting monomer. More specifically, the Arg411 residue in the C-terminal tail of a monomer formed salt bridges with the carboxylate group of OAA in the active site of the contacting monomer (Supplementary Fig. S1).

Consistent with the analytical ultracentrifugation results, the assembly analysis based on PDBePISA showed the dissociation of 9.7 kcal/mol of free energy following hexamer assembly, indicating that the hexamer is thermodynamically stable [12]. The triangle-like hexamer was generated by an approximate 3-fold operation of the dimers. This dimer–dimer interface region had two binding sites. The loop α4/α5 was involved in interaction site 1 with an area of ~410 Å^2, whereas loops α8/α9 and α9/α10 were mainly involved in interface site 2, with a binding area of ~500 Å^2 (Fig. 2). During the development of the model and the refinement processes, the electron density of citrate was initially detected near the active site in the citrate-bound *Hy*CS structure. Even when citrate was not added as a ligand during the preparation of protein samples, the crystal precipitant solution was found to contain 1 M sodium citrate. Because of this, we identified a distinct electron density map in the active site, with citrate fitting well into the electron density map. The citrate-bound active site was composed of the α10–α11, α12–α13, and α14–α15 loops, as well as α17 and α18 helical regions containing the His266, His308, and Asp366 catalytic residues. Furthermore, the bound citrate tightly interacted with positively charged residues and several histidine residues at the active site. In particular, the His231, His266, His308, Arg317, and Arg391 residues were seen to interact with the oxygen atoms of the citrate molecule. These ligand-binding residues were found to be highly conserved in all type II CSs.

Table 1
X-ray diffraction data collection and refinement statistics.

	Citrate bound *Hy*CS
Data set	
X-ray source	PAL 5C beam line
Space group	$C222_1$
Unit-cell parameters (Å, °)	a = 134.3, b = 166.2, c = 135.3 α = β = γ = 90
Wavelength (Å)	1.2823
Resolution (Å)	50.00–2.20 (2.24–2.20)
Total reflections	610,837
Unique reflections	76,885 (3807)
Average I/σ (I)	47.2 (8.1)
R_{merge}[a]	0.073 (0.342)
Redundancy	7.9 (8.2)
Completeness (%)	99.8 (100.0)
Refinement	
Resolution range (Å)	41.55–2.20 (2.23–2.20)
No. of reflections of working set	76,818 (2578)
No. of reflections of test set	3848 (162)
No. of amino acid residues	1292
No. of water molecules	399
R_{cryst}[b]	0.190 (0.222)
R_{free}[c]	0.235 (0.258)
R.m.s. bond length (Å)	0.008
R.m.s. bond angle (°)	0.853
Average B value (Å^2) (protein)	49.10
Average B value (Å^2) (solvent)	41.67

Values in parentheses refer to highest resolution shells.
[a] $R_{merge} = \sum|<I> - I|/\sum<I>$.
[b] $R_{cryst} = \sum||Fo| - |Fc||/\sum|Fo|$.
[c] R_{free} calculated with 5% of all reflections excluded from the refinement stages using high-resolution data.

2.2. Structural comparison of HyCS with other type II CS structures

Structural comparisons between *Hy*CS and *Ec*CS revealed significant conformational changes in the small-domain region. When the structure of *Hy*CS was superimposed onto the *Ec*CS structure [6] (PDB code 4G6B), significant differences were observed at the His266 residue in *Hy*CS (His264 in *Ec*CS). Whereas the His266 residue interacted with bound citrate in the HyCS structure, the corresponding His264 residue of *Ec*CS interacted with Trp260 in the inactive (unliganded open) state (Fig. 3A). Notably, we identified this interaction between histidine and tryptophan in all other inactive type II CS structures (Table 2). However, the histidine residue in the active (liganded closed) type II CS structures always formed a specific interaction with the bound ligand [8,11]. Thus, ligand binding might result in the release of the face-to-edge interaction between His266 and Trp262. Moreover, this ligand binding-induced conformational change might be closely related to the cooperative ligand binding of the other subunit. Our structural superposition results for the *Hy*CS dimer and *Ec*CS structure revealed that the inactive structure of *Ec*CS had a structural clash with subunit B of *Hy*CS. Thus, we assumed that small domain conformational changes followed by citrate binding might induce and transfer further structural changes to other subunits [6,7] (Fig. 3B).

2.3. Cooperativity of substrate binding and allosteric inhibition of HyCS

Rearrangement of the small domain upon ligand binding in subunit A has been suggested to affect the formation of the next ligand-binding sites in hexameric *Hy*CS [9]. In our activity assay experiment using the W262A mutant, we found that the mutation resulted in an increased Hill coefficient of 2.4, which was comparable to that of wild-type *Hy*CS. Thus, we considered that the tight interaction between His266 and Trp262 might prohibit and lock the cooperativity of *Hy*CS. However, as ligand binding is known to cause a conformational change in the small domain, this might thus increase the affinity of the second active site for its substrate by relieving the interaction between His266 and Trp262. Accordingly, the W262A mutant would accommodate the ligand more easily than the wild-type protein without an allosteric activator. Therefore, we assumed that the W262A mutant protein might mimic the activated state of type II CS via an allosteric activator (Fig. 4).

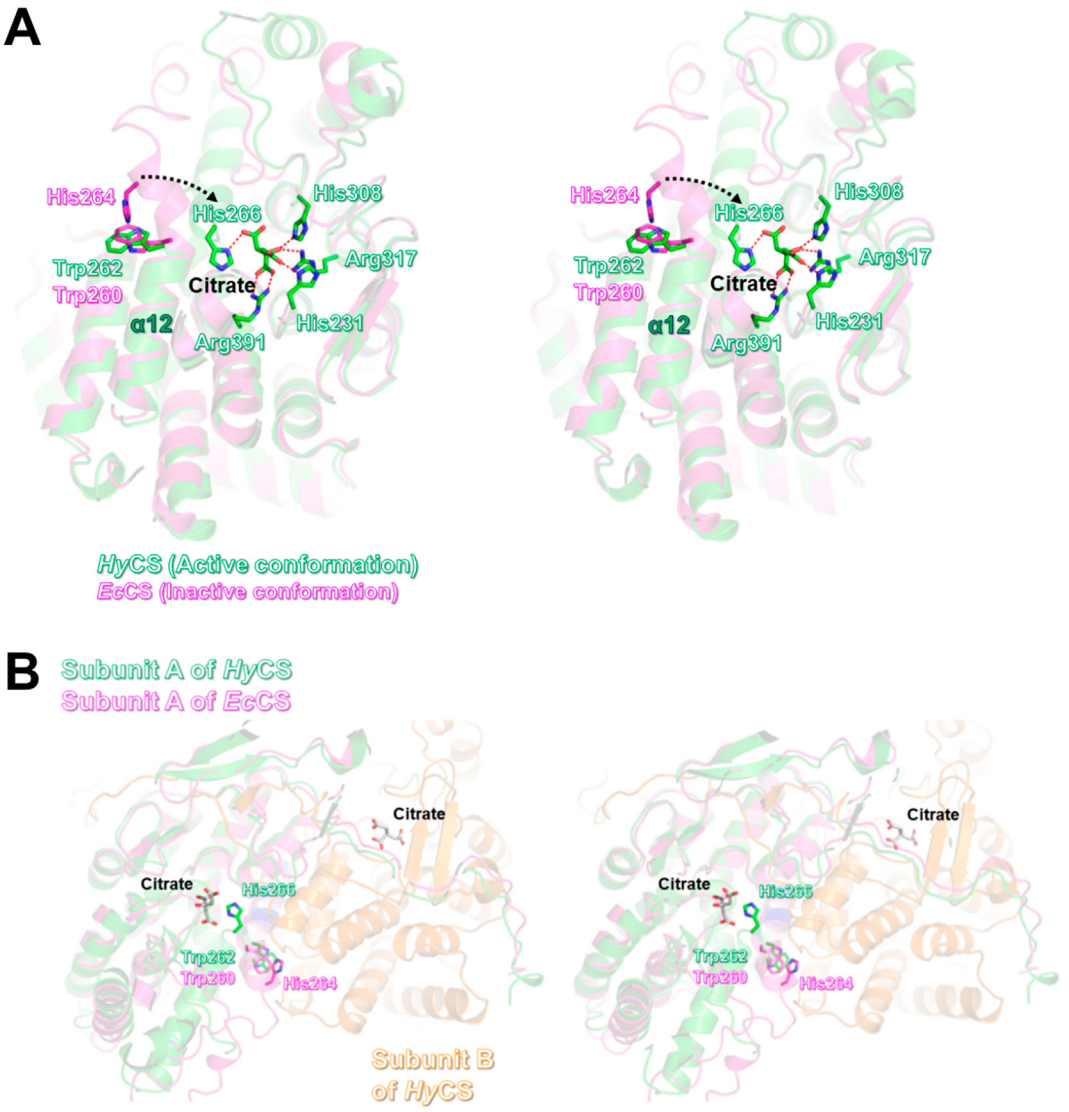

Fig. 3. Structural comparison of *Hy*CS and *Ec*CS. (A) Stereo view of the superimposed structures of citrate-bound *Hy*CS (closed conformation) and apo-*Ec*CS (open conformation, PDB code: 4G6B) shows that the His266 residue (His264 in *Ec*CS) underwent a conformational change upon citrate binding. The His264 and Trp260 residues showed a face-to-edge interaction in the open state structure of *Ec*CS. (B) Stereo view of the superimposed structures of monomer *Ec*CS and dimer *Hy*CS showed steric hindrance with the other subunit of *Hy*CS. This indicated that the citrate binding-induced conformational changes result in the transfer of further structural changes to other subunits.

Type II CSs are allosterically inhibited by NADH, ATP, and citrate. Two NADH-bound *Ec*CS structures (PDB codes 1NXG and 1OWB) were previously determined [6,7,13]. In these studies, it was reported that NADH bound to the dimer-dimer interfaces in the NADH-bound EcCS structures. To investigate the inhibitory properties of *Hy*CS, we performed an activity assay by adding NADH, ATP, or citrate. Our kinetic

Table 2
Known type II citrate synthase structures and analysis of small domain conformation.

Protein name	*Hy*CS	*Ec*CS					*Aa*CS	*Mt*CS
PDB code	7E8N	4G6B[a] (1K3P)	1NXE	1NXG	1OWC	1OWB	2H12	4TVM
Source	*Hymenobacter* sp. PAMC 26554	*Escherichia coli*	*Escherichia coli*	*Escherichia coli*	*Escherichia coli*	*Escherichia coli*	*Acetobacter aceti*	*Mycobacterium tuberculosis*
UniProtKB code	A0A142HAE2	P0ABH7					P20901	P9WPD5
Sequence identity/similarity (%) with *Hy*CS				48/67			52/68	57/74
Complexed ligand	Citrate	Sulfate ion	Sulfate ion	Sulfate ion, NADH	Sulfate ion	Sulfate ion, NAD	Sulfate ion, oxaloacetate and carboxymethyldethia coenzyme A (CMX)	Oxaloacetate
Conformation	Closed	Open	Open	Open	Open	Open	Closed	Closed

[a] Entry 4G6B supersedes 1K3P.

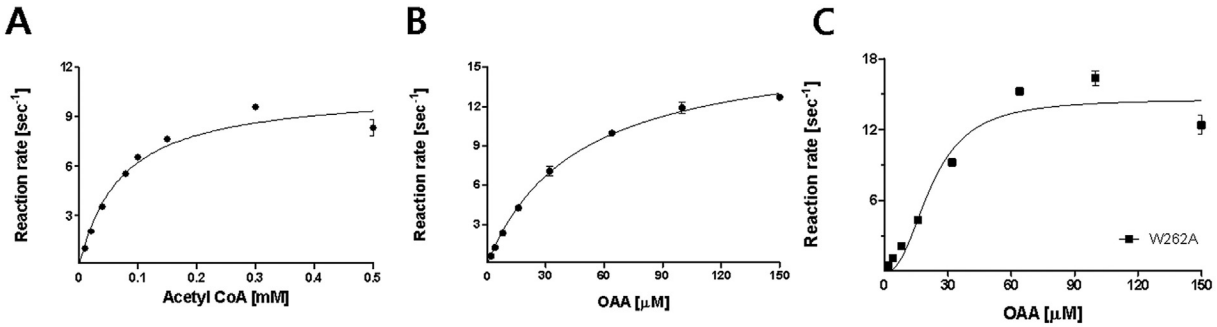

D

	Substrate	K_M, μM	k_{cat}, s^{-1}	k_{cat}/K_M, $s^{-1}\mu M^{-1}$	n (Hill parameter for OAA)
WT	Acetyl-CoA	71.2 ± 10.4	10.7 ± 0.5	0.15	1.3
	Oxaloacetate	45.7 ± 2.4	17.0 ± 0.3	0.37	1.1
W262A	Oxaloacetate	32.0 ± 11.0	18.1 ± 1.9	0.57	2.4

Fig. 4. Kinetic data for wild-type and W262A mutant of *Hy*CS. Michaelis-Menten kinetics graph of *Hy*CS wild-type for (A) oxaloacetate and (B) acetyl-CoA. (C) Positive cooperativity of the W262A HyCS mutant. (D) Values of K_M, k_{cat}, catalytic efficient (k_{cat}/K_M), and Hill parameters for wild-type and W262A mutant *Hy*CS.

analysis data showed that the activity of *Hy*CS was significantly inhibited by a high concentration (200 μM) of citrate, which is a typical feedback inhibition by the end product. In contrast, we noted that the activity of *Hy*CS was not affected by NADH (Fig. 5). It should be noted that we tried to obtain reasonable kinetic as well as Hill parameters using the W264A mutant and acetyl-CoA substrate. However, we could not get obvious and specific parameters. The W264A mutant showed about three-times reduced activity compared with the wild-type protein. We suspect that the W264A mutant is probably very sensitive to feedback inhibition by the generated citrate as illustrated in Fig. 5A.

Structural comparison between the *Hy*CS and NADH-bound *Ec*CS structures (PDB code: 1NXG) showed that the NADH-binding pocket structures were similar. In addition, we found that several NADH-interacting residues were conserved between *Hy*CS and *Ec*CS (*Ec*CS numbering in parentheses): Lys110 (Arg109), His111 (His110), Leu113 (Met112), His115 (His114), Tyr146 (Tyr145), Leu161 (Ile159), and Arg165 (Arg163) (Fig. 6A). However, significant conformational changes were detected in the interface region between the two dimers in the *Hy*CS hexamer structure. More specifically, we observed that the α9/10 loop region from the neighboring subunit of *Hy*CS occupied the NADH-binding pocket with a bulky amino acid (Phe206 – Tyr211). Because of this spatial restriction, we considered that NADH might not bind to *Hy*CS to exert its inhibitory activity.

Additionally, this α9/10 loop region appeared to be a unique feature of type II CSs. Sequence alignment showed that the hexameric type II CSs had an additional amino sequence, whereas dimeric Type I CSs did not. Together, these findings suggested that NADH-mediated allosteric inhibition of the remote active site is initiated by blocking the critical region for the oligomeric state of type II CSs. However, no information on the inhibitory mechanism of type I CSs by NADH supports this hypothesis (Fig. 6B). In addition, we tested the inhibition by ATP in *Hy*CS, but our results were not interpretable because of the high salt impurities in the ATP sample. As described above, type II CSs are known to be activated by various salt ions, such as KCl.

In conclusion, we report the first crystal structure of *Hy*CS from the psychrophilic *Hymenobacter* sp. PAMC 26554 [10]. Our structural and biochemical analyses revealed that the face-to-edge interaction between His266 and Trp262 is important for the control of the ligand cooperative binding of *Hy*CS. The diversification pattern of CS in the phylogenetic tree generated using the full CS sequences from various organisms is consistent with the categorization of CS based on the amino acid identity at position 262. The Trp262 residue of *Hy*CS is strictly conserved in other type II CSs. This residue is replaced by Lys residue in the groups of thermophilic archaea and bacteria (PDB codes 1AJ8, 1VGP, 1IOM, and 2P2W). Eukaryotic mammalian type I CSs (PDB codes 6K5V, 5UZR, 1AMZ, and 1CTS) commonly contain an Ala residue at the position corresponding to Trp262 of *Hy*CS. Intriguingly, CS from the pathogenic bacterium, *Mycobacterium tuberculosis* (PDB code 3HWK), has a Lys residue at the position corresponding to Trp262 of *Hy*CS but that from the *Mycobacterium tuberculosis* variant bovis AF2122/97 (PDB code 6WGY) contains a Ser residue instead of Lys (Supplementary Fig. S2).

Furthermore, we found that the unique amino acid sequence of *Hy*CS on the dimer-dimer interface might interrupt NADH binding; thus, *Hy*CS is not subject to NADH-mediated inhibition. Our results provided an insight into the factors that determine the allosteric control and ligand cooperative binding of all type II CSs, as well as *Hy*CS.

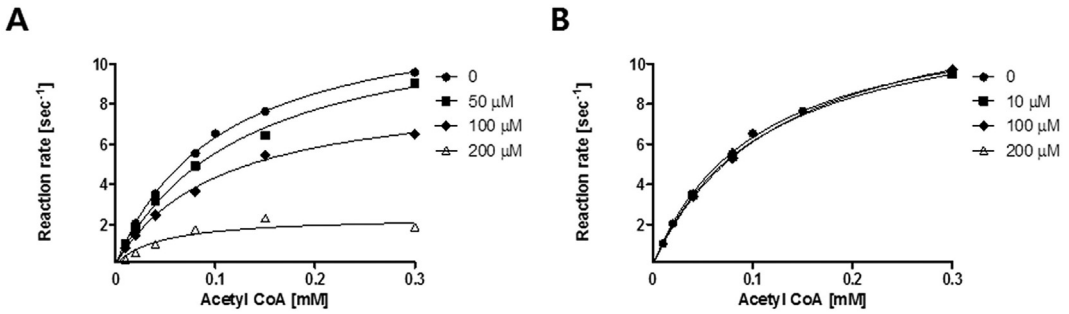

Fig. 5. Inhibition studies of *Hy*CS. Kinetic analysis for the inhibition of wild-type *Hy*CS by (A) citrate and (B) NADH at different concentrations of acetyl-CoA.

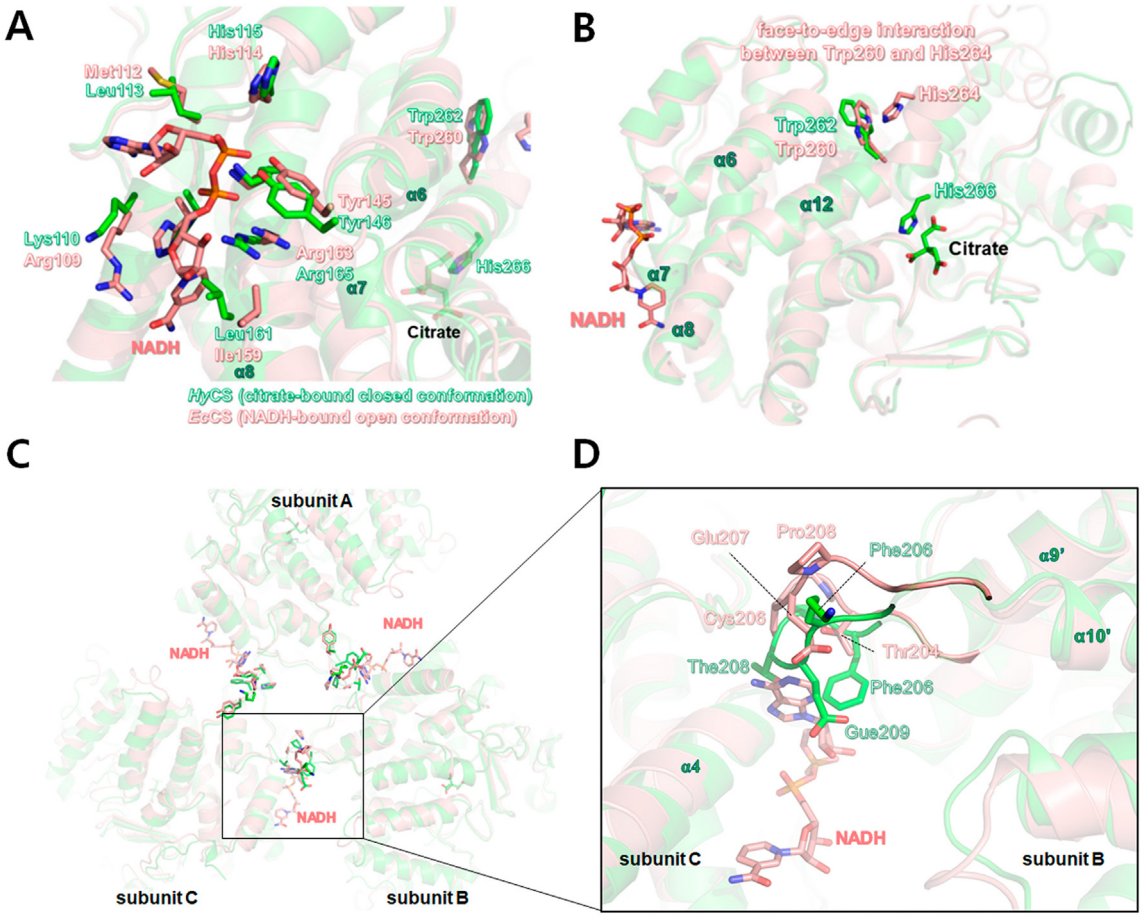

Fig. 6. Comparison of NADH binding sites of *Hy*CS and *Ec*CS. (A, B) Stereo view of the superimposed structures of citrate-bound *Hy*CS (closed conformation) and NADH-bound *Ec*CS (open conformation, PDB code: 1NXG). (C, D) Spatial restriction of NADH binding on the α9/10 loop by bulky residues from the neighboring subunit. *Ec*CS structure and NADH are colored pink. *Hy*CS is colored green. The residues of the α9/10 loop are represented in sticks with CPK colors.

3. Materials and methods

3.1. Cloning, expression, and purification of HyCS

The open reading frame of the *CS* gene from *Hymenobacter* sp. PAMC 26554, which is 431 bp in length, was retrieved from the database of the National Center for Biotechnology Information (accession no.: WP_068332949). The *Hy*CS gene codon was optimized according to the codon usage bias in *E. coli*. The sequence was synthesized and subcloned between the *Nde*I and *Xho*I sites of pET-28a(+) (Novagen, Madison, WI, USA) and transformed into *E. coli* BL21(DE3) (Supplementary Table S1). Cells were grown at 37 °C in 2 L Luria–Bertani medium supplemented with 50 μg mL^{-1} kanamycin until an OD_{600} of 0.6 was reached. The *Hy*CS protein was expressed overnight in the presence of isopropyl-1-thio-β-D-galactopyranoside at a final concentration of 0.4 mM at 25 °C. Bacterial cells were harvested by centrifugation and then suspended in lysis buffer (50 mM sodium phosphate, 300 mM NaCl, and 5 mM imidazole (pH 8.0) supplemented with 0.2 mg/ mL lysozyme). Cells were disrupted by sonication, and cell debris was removed by centrifugation (2570 ×*g* for 1 h at 4 °C). The supernatant was applied to a Ni-NTA column (Qiagen, Hilden, Germany) equilibrated with the lysis buffer. After washing of column with 50 mM sodium phosphate buffer containing 300 mM NaCl and 20 mM imidazole (pH 8.0), bound proteins were eluted with 300 mM imidazole buffer. The N-terminal His-tag was removed by treatment with thrombin and purified by size exclusion chromatography using a Superdex 200 column (GE Healthcare, Piscataway, NJ, USA) equilibrated in 50 mM Tris-HCl (pH 8.0) and 150 mM NaCl. Final purified proteins were verified using sodium dodecyl sulfate (SDS)-polyacrylamide gel electrophoresis (Supplementary Fig. S3).

3.2. Analytical ultracentrifugation

To investigate the oligomeric state of *Hy*CS in solution, analytical ultracentrifugation was performed using a ProteomeLab XL-A (Beckman Coulter, Brea, CA, USA) in buffer conditions of 150 mM NaCl and 20 mM Tris-HCl (pH 8.0) at 20 °C. The sample was centrifuged at 14,225 ×*g* for 10 min, and the sedimentation profile was monitored at a wavelength of 280 nm. Data were analyzed using the SEDFIT program [14].

3.3. Enzymatic activity assay

CS catalyzes the formation of citrate and free CoA from oxaloacetate and acetyl-CoA. Steady-state kinetic studies of the wild-type and W262A mutant *Hy*CS were performed in the presence of the KCl (0.1 M) allosteric activator at 30 °C. The standard reaction mixture contained 100 mM Tris-HCl (pH 8.0), 0.1 M KCl, 0.2 mM DTNB, and appropriate concentrations of oxaloacetate and acetyl-CoA. For the kinetic studies of oxaloacetate, the concentration of oxaloacetate varied from 2 to 150 μM at a fixed concentration of acetyl-CoA (300 μM). For the kinetic studies of acetyl-CoA, the concentration of acetyl-CoA varied from 10 to 500 μM at a fixed concentration of oxaloacetate (100 μM). Enzymatic reactions were started by adding 0.5 μg *Hy*CS enzyme. Enzymatic

activities were measured spectrophotometrically by monitoring the increase in absorbance at 412 nm (extinction coefficient of 14,200 $M^{-1}\cdot cm^{-1}$). To assess the cooperativity of the catalytic activity of the W262A *Hy*CS mutant, we performed a Hill analysis of the oxaloacetate concentration dependence of HyCS activity in the presence of 300 μM acetyl-CoA. All data were fitted to Michaelis-Menten or Hill equations using the GraphPad Prism 5.02 software (GraphPad, Inc., San Diego, CA, USA). For the enzymatic inhibition assay, we performed a kinetic analysis of acetyl-CoA using different concentrations of citrate, NADH, and ATP.

The reverse reaction of *Hy*CS was measured in combination with malate dehydrogenase as the citrate- and CoA-dependent oxidation of NADH. The reverse reaction mixture contained 100 mM Tris-HCl (pH 8.0), 5 mM $MgCl_2$, 0.5 mM CoA, 0.5 mM NADH, 10 U mL^{-1} malate dehydrogenase (Sigma M1576, St. Louis, MO, USA), and 1 mM citrate. The reaction was started by adding 1 mg *Hy*CS, and the activity was measured spectrophotometrically at 365 nm (extinction coefficient of 3400 $M^{-1}\cdot cm^{-1}$).

3.4. Crystallization and data collection

Initial crystallization screening for *Hy*CS was performed using the sitting-drop vapor-diffusion method in 96-well sitting-drop plates (Emerald Bio, Bainbridge Island, WA, USA) incubated at 293 K. Crystallization drops were set up using a mosquito crystallization robot (STP Labtech, Hertfordshire, UK) with several commercially available crystallization solution kits, including the MCSG I-IV (Microlytic, Burlington, MA, USA), Index, and SaltRx (Hampton Research, Aliso Viejo, CA, USA). Each drop consisted of 300 nL protein solution and 300 nL crystallization solution, equilibrated against 80 μL of reservoir solution. Crystals of citrate-bound *Hy*CS were obtained from 0.1 M sodium cacodylate:HCl (pH 6.5) and 1 M sodium citrate tribasic (MCSG III #A1). Single crystals of both forms were harvested and briefly soaked in Paratone-N oil (Hampton Research) for cryopreservation. Complete data sets were collected on the BL-5C beamline of the Pohang Accelerator Laboratory (Pohang, Korea). The dataset for citrate-bound *Hy*CS containing 200 images was collected over an oscillation range of 1° per image with 1 s exposure. Data were processed and scaled using the HKL-2000 software [15]. Detailed X-ray diffraction data collection statistics are presented in Table 1.

3.5. Structure determination and refinement

The crystal structure of citrate-bound *Hy*CS was determined at 2.2 Å resolution by molecular replacement using the program *MOLREP* from the *CCP4i* suite [16,17]. The structure of CS from *M. tuberculosis* (PDB code: 4TVM), which has 58% amino acid sequence identity with *Hy*CS, was used as the search model. The model was rebuilt and refined using *COOT* [18] and *REFMAC5* [19]. The *phenix.refine* program of the PHENIX suite was also used for model refinement [18]. The final model of the citrate-bound *Hy*CS structure showed an R_{cryst} of 0.190 and R_{free} of 0.235, with a total of 1292 amino acid residues and 394 water molecules. The quality of the final structural model was checked using the *MolProbity* structure validation server [20]. The structural model and reflection data were deposited in the Protein Data Bank under the accession code 7E8N. All refinement statistics are presented in Table 1. PyMOL was used for visualization and production of figs. [21].

Supplementary data to this article can be found online at https://doi.org/10.1016/j.ijbiomac.2021.04.141.

CRediT authorship contribution statement

Conceptualization: J.H.L. and S—S.C. Investigation; S—H.P., C.W.L., D—W.B., H.D., C—S.J. and J.H.. Writing – Original Draft; S—H.P., C.W.L., and D—W.B. Writing – Review & Editing; H.D., S.-S.C., and J.H.L. All authors discussed the results, commented on the manuscript, and approved the final version.

Declaration of competing interest

The authors declare no conflicts of interest.

Acknowledgements

We thank the staff at the X-ray core facility of the Korea Basic Science Institute (Ochang, Korea) and BL-5C of the Pohang Accelerator Laboratory (Pohang, Korea) for their assistance with data collection. This research was a part of the project titled “Development of potential antibiotic compounds using polar organism resources (15250103, KOPRI Grant PM21030)” funded by the Ministry of Oceans and Fisheries, Korea. This research was also supported by a National Research Foundation of Korea Grant from the Korean Government (MSIT; the Ministry of Science and ICT) (NRF-2017M1A5A1013568) (KOPRI-PN20082) (Title: Application study on the Arctic cold-active enzyme degrading organic carbon compounds).

Data availability

Atomic coordinates and structure factors for the citrate-bound *Hy*CS structure were deposited in the PDB under accession code 7E8N.

References

[1] S.J. Remington, Structure and mechanism of citrate synthase, Curr. Top. Cell. Regul. 33 (1992) 209–229.
[2] G.S. Bell, R.J. Russell, H. Connaris, D.W. Hough, M.J. Danson, G.L. Taylor, Stepwise adaptations of citrate synthase to survival at life's extremes. From psychrophile to hyperthermophile, Eur. J. Biochem. 269 (2002) 6250–6260.
[3] G. Wiegand, S.J. Remington, Citrate synthase: structure, control, and mechanism, Annu. Rev. Biophys. Biophys. Chem. 15 (1986) 97–117.
[4] C.M. Smith, J.R. Williamson, Inhibition of citrate synthase by succinyl-CoA and other metabolites, FEBS Lett. 18 (1971) 35–38.
[5] N.T. Nguyen, R. Maurus, D.J. Stokell, A. Ayed, H.W. Duckworth, G.D. Brayer, Comparative analysis of folding and substrate binding sites between regulated hexameric type II citrate synthases and unregulated dimeric type I enzymes, Biochemistry 40 (2001) 13177–13187.
[6] D.J. Stokell, L.J. Donald, R. Maurus, N.T. Nguyen, G. Sadler, K. Choudhary, P.G. Hultin, G.D. Brayer, H.W. Duckworth, Probing the roles of key residues in the unique regulatory NADH binding site of type II citrate synthase of Escherichia coli, J. Biol. Chem. 278 (2003) 35435–35443.
[7] R. Maurus, N.T. Nguyen, D.J. Stokell, A. Ayed, P.G. Hultin, H.W. Duckworth, G.D. Brayer, Insights into the evolution of allosteric properties. The NADH binding site of hexameric type II citrate synthases, Biochemistry 42 (2003) 5555–5565.
[8] J.A. Francois, C.M. Starks, S. Sivanuntakorn, H. Jiang, A.E. Ransome, J.W. Nam, C.Z. Constantine, T. Joseph Kappock, Structure of a NADH-insensitive hexameric citrate synthase that resists acid inactivation, Biochemistry 45 (2006) 13487–13499.
[9] H.W. Duckworth, W. Harry, T.N. Nham, Y. Gao, L.J. Donald, R. Maurus, A. Ayed, B. Bruneau, G.D. Brayer, Enzyme–substrate complexes of allosteric citrate synthase: evidence for a novel intermediate in substrate binding, Biochim. Biophys. Acta 1834 (2013) 2546–2553.
[10] T.J. Oh, S.R. Han, D.H. Ahn, H. Park, A.Y. Kim, Complete genome sequence of *Hymenobacter* sp. strain PAMC26554, an ionizing radiation-resistant bacterium isolated from an Antarctic lichen, J. Biotechnol. 227 (2016) 19–20.
[11] D.M. Ferraris, R. Spallek, W. Oehlmann, M. Singh, M. Rizzi, Structures of citrate synthase and malate dehydrogenase of *Mycobacterium tuberculosis*, Proteins 83 (2015) 389–394.
[12] E. Krissinel, K. Henrick, Inference of macromolecular assemblies from crystalline state, J. Mol. Biol. 372 (2007) 774–797.
[13] S.H. Lee, H.F. Son, K.J. Kim, Structural insights into the inhibition properties of archaeon citrate synthase from *Metallosphaera sedula*, PLoS One 14 (2019), e0212807, .
[14] P. Schuck, M.A. Perugini, N.R. Gonzales, G.J. Howlett, D. Schubert, Size-distribution analysis of proteins by analytical ultracentrifugation: strategies and application to model systems, Biophys. J. 82 (2002) 1096–1111.
[15] Z. Otwinowski, W.I. Minor, C.W. Carter Jr., R.M. Sweet, Methods in enzymology, Macromolecular Crystallography, Part A, vol. 276, Elsevier, New York, 2009.
[16] A. Vagin, A. Teplyakov, Molecular replacement with MOLREP, Acta Crystallogr., Sect. D: Biol. Crystallogr. 66 (2010) 22–25.
[17] M.D. Winn, C.C. Ballard, K.D. Cowtan, E.J. Dodson, P. Emsley, P.R. Evans, R.M. Keegan, E.B. Krissinel, A.G.W. Leslie, A. McCoy, S.J. McNicholas, G.N. Murshudov, N.S. Pannu, E.A. Potterton, H.R. Powell, R.J. Read, A. Vagin, K.S. Wilson, Overview of the CCP4

suite and current developments, Acta Crystallogr., Sect. D: Biol. Crystallogr. 67 (2011) 235–242.
[18] P. Emsley, K. Cowtan, Coot: model-building tools for molecular graphics, Acta Crystallogr., Sect. D: Biol. Crystallogr. 60 (2004) 2126–2132.
[19] G.N. Murshudov, P. Skubák, A.A. Lebedev, N.S. Pannu, R.A. Steiner, R.A. Nicholls, M.D. Winn, F. Long, A.A. Vagin, REFMAC5 for the refinement of macromolecular crystal structures. Acta Crystallogr. D. Biol, Crystallogr 67 (2011) 355–367.
[20] V.B. Chen, W.B. Arendall, J.J. Headd, D.A. Keedy, R.M. Immormino, G.J. Kapral, L.W. Murray, J.S. Richardson, D.C. Richardson, MolProbity: all-atom structure validation for macromolecular crystallography, Acta Crystallogr., Sect. D: Biol. Crystallogr. 66 (2010) 12–21.
[21] W.I. DeLano, The PyMOL Molecular Graphics System, DeLano Scientific, San Carlos, 2002.